In-Loop Mechanical Screening for Multiphysics Multi-Objective Electric Motor Optimization

Federico Valpiani
Department of Energy
Politecnico di Milano
Milan, Italy
federico.valpiani@polimi.it

Alessandro Niccolai
Department of Energy
Politecnico di Milano
Milan, Italy
alessandro.niccolai@polimi.it

Sonia Leva
Department of Energy
Politecnico di Milano
Milan, Italy
sonia.leva@polimi.it

***Abstract*—Multi-objective optimization of electric motors based solely on electromagnetic criteria neglects structural constraints, yielding Pareto-optimal solutions that may be mechanically infeasible. This paper presents a multiphysics, multi-objective framework for IPMSM rotor design, where electromagnetic and structural analyses are coupled within the same evolutionary loop to enforce mechanical admissibility. The rotor geometry, defined by a 52-parameter asymmetric double-layer V-shaped configuration, is optimized to maximize torque and minimize torque ripple at two operating speeds. Electromagnetic performance is evaluated via finite elements, while structural feasibility is assessed in-loop under overspeed through a stress-based criterion. Results show that neglecting mechanical constraints distorts the Pareto front: 32% of solutions from electromagnetic-only optimization are infeasible a posteriori, indicating that post-processing is insufficient. The admissible front instead comprises physically realizable designs with improved performance near structural limits.**

***Index Terms*—Interior Permanent Magnet Synchronous Motor (IPMSM), Multi-objective optimization, Multiphysics finite-element analysis, NSGA-II**

I. Introduction

The design of electric machines involves multiple, often conflicting, performance requirements combined with industrial constraints [1]. In practical applications, electric motors must ensure high torque with low ripple across operating conditions while satisfying manufacturability, mechanical integrity, and reliability limits [2]. This leads to a multi-objective constrained optimization problem, where electromagnetic performance must be balanced against feasibility constraints.

Multi-objective evolutionary algorithms are widely adopted in this context due to their ability to handle non-linear and conflicting objectives. Methods such as NSGA-II are commonly coupled with finite element analyses to accurately evaluate candidate solutions. Prior works have applied these approaches to motor optimization, including electromagnetic–thermal integration [3], performance-driven design of permanent magnet machines [4], [5], and hybrid frameworks with surrogate models [6]–[8]. Open-source environments have also been proposed to support industrial design trade-offs [9].

However, electromagnetic-focused frameworks show limitations in industrial practice. Mechanical aspects are often represented through simplified geometric constraints, which exclude clearly infeasible designs but do not guarantee structural integrity, especially for advanced rotor topologies [10]. This may lead to overstressed regions or the exclusion of feasible solutions, particularly in high-performance designs where small geometric variations strongly affect stress distribution [11]. To overcome these issues, recent studies have introduced multiphysics optimization approaches that couple electromagnetic and mechanical analyses [12]. In such frameworks, mechanical stress is evaluated via finite element methods and treated as a constraint or objective [13], with extensions to surrogate-assisted optimization under heterogeneous evaluation costs [14].

In contrast, this study embeds structural admissibility within the evolutionary loop and focuses on industrial rotor geometries. The main contributions are: (i) an in-loop mechanical screening framework coupling structural and electromagnetic finite element analyses; (ii) a comparative assessment of optimization with and without mechanical evaluation, quantifying effects on Pareto front topology and feasibility; and (iii) a cluster-based analysis identifying rotor regions prone to mechanical overstress.

II. Problem Definition

The motor topology and requirements were defined in collaboration with Mavel EDT., an Italian company specialized in electric motors and inverters for high-performance premium traction applications. The framework is applied to a validated Interior Permanent Magnet Synchronous Motor (IPMSM), with optimization formulated as rotor fine-tuning to reduce torque ripple while preserving maximum torque. The baseline geometry (Fig. 1), has asymmetric double-layer V-shaped magnet configuration, with initial performance shown in Tab. I.

Due to the asymmetric layout, each magnet layer is parameterized independently through: (i) magnet thickness and length; (ii) magnet orientation; (iii) x and y coordinates of the magnet center; (iv) x and y coordinates of two control points used to parameterize the outer flux-barrier shape; (v) x and y coordinates of two control points used to parameterize the inner flux-barrier shape. Overall, each magnet layer is described by 13 independent geometric variables. As a result, a four-layer configuration is defined by 52 design parameters.

This work was supported by Mavel EDT. through an industrial Ph.D. sponsorship.

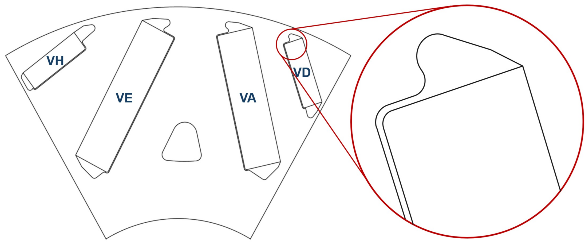

Fig. 1. Precursor rotor geometry used as baseline for the optimization. The permanent-magnet layers are labeled VA, VD, VE, and VH.

TABLE I. Performance of the precursor configuration

Name	Symbol	Value
Number of poles	N_p	6
Number of slots	N_s	36
Torque Average at EMAG-A	T_{nom}	275.8 Nm
Torque Ripple at EMAG-A	T_{rip}	11.9 %
Torque Average at EMAG-B	T_{avg}	46.7 Nm
Torque Ripple at EMAG-B	T_{rip}	16.3 %
Magnet mass	w_{mag}	1.54 kg
Total Harmonic Distortion	THD	8.4 %

III. Methodology

The proposed framework evaluates each candidate through a staged pipeline (see Fig. 2), where simulations stages of increasing computational cost are sequentially executed: geometrically or structurally infeasible designs are discarded early, while candidates reaching electromagnetic analysis are penalized if performance thresholds are not met. This section first presents the optimization algorithm and initialization strategy, followed by the objective definition and electromagnetic evaluation. The constraint architecture is then introduced, including geometric feasibility and the MECH-ON/MECH-OFF logic for enforcing structural admissibility. The in-loop mechanical evaluation and the penalty strategy for infeasible or low-performance solutions are finally described.

A. Optimization Algorithm and Population Initialization

The optimization employs a custom multi-objective genetic algorithm in MATLAB, based on NSGA-II [15] for its effectiveness on non-convex Pareto fronts. The population consists of 100 individuals, with a maximum of 5000 fitness evaluations. Offspring are generated via two-point crossover with roulette-wheel selection, while mutation uses a Gaussian operator (10% probability, 10% amplitude). Algorithm parameters are fixed based on prior studies on similar IPMSM topologies. To assess variability, ten independent runs are performed with different random seeds under identical settings.

Particular attention is given to population initialization, as the optimization targets refining a motor already satisfying design requirements. The process is therefore formulated as a local geometric refinement.

The parametric design core includes a file-based parser that extracts design variables from the precursor FEMM model, used as the reference configuration. The initial population is generated by applying zero-mean Gaussian perturbations with a standard deviation of 0.5% of each nominal value. The corresponding performance metrics are reported in Table I.

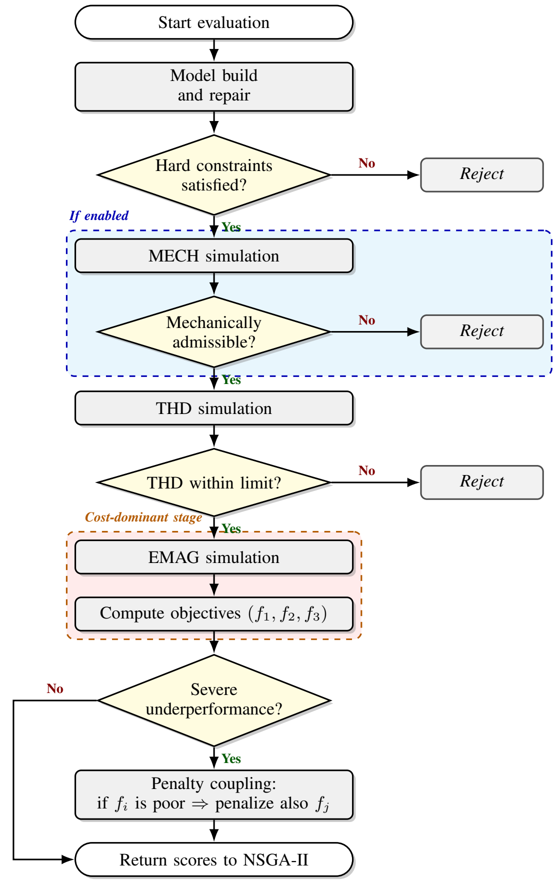

Fig. 2. Multi-stage fitness evaluation with early rejection and penalty coupling.

TABLE II. EMAG operating points

	Max Torque	Max Speed
Current*	1	0.5
Speed*	1	4
Objective	Maximize T_{nom} [Nm] Minimize T_{rip} [%]	Minimize T_{rip} [%]
Reference	EMAG-A	EMAG-B

*Quantities are normalized with respect to Max Torque simulation point.

B. Objectives and Electromagnetic Simulation

The optimization targets rotor geometry, aiming to maximize nominal torque T_{nom} and minimize torque ripple T_{rip}. For consistency, objectives are expressed in minimization form, with torque defined as $-T_{\text{nom}}$. The objectives are evaluated at two operating points, (Table II). The first point (EMAG-A), defined at the maximum-torque condition, is used to assess both average torque and ripple. The second (EMAG-B), defined at maximum speed, targets torque ripple under high-speed operation. This formulation captures both torque capability and quality across the main operating regimes.

For each operating point, the torque waveform is obtained from finite element simulations at multiple rotor positions.

To reduce computational cost, only one-third of the geometry is modeled by exploiting symmetry; further reduction is not possible due to the asymmetric pole configuration. The rotor position is discretized over $60°$ with $n_{\text{step}} = 20$ simulations per operating condition.

Electromagnetic analyses are performed using the open-source Finite Element Method Magnetics (FEMM) software [16]. For each rotor position, the electromagnetic torque T_i is computed using the Weighted Stress Tensor Method [17]. The nominal torque is defined as the average value of the torque waveform:

$$T_{\text{nom}} = \frac{1}{n_{\text{step}}} \sum_{i=1}^{n_{\text{step}}} T_i \tag{1}$$

while the torque ripple is defined as the normalized peak-to-peak torque variation:

$$T_{\text{rip}} = \frac{\max(T_i) - \min(T_i)}{T_{\text{nom}}} \cdot 100 \tag{2}$$

This problem formulation ensures that each candidate solution is evaluated consistently through a multi-position electromagnetic analysis, capturing both average performance and torque smoothness.

In addition to the primary objectives T_{nom} and T_{rip}, the optimization process also monitors complementary performance indicators and constraint-related quantities that are relevant for industrial decision-making: the magnet mass w_{mag}, and the Total Harmonic Distortion (THD).

The electromotive force THD is imposed as an optimization constraint. It is obtained from a single no-load FEMM analysis, with the waveform sampled in the air gap. After Fourier decomposition, the THD is computed as the root-mean-square ratio of the first $N = 100$ harmonics to the fundamental component:

$$\text{THD} = \frac{\sqrt{\sum_{i=2}^{N} E_i^2}}{E_1} \cdot 100 \tag{3}$$

where E_1 is the fundamental component and E_i the higher-order harmonics. For this evaluation, the stator is replaced by a homogeneous iron sector to isolate rotor-induced harmonics. This choice excludes distortions due to stator slotting and other stator-related effects.

C. Constraints Architecture

Geometric and manufacturability constraints are organized into two distinct levels, depending on whether mechanical screening is enabled.

1) First level: is always active and includes geometric feasibility and material usage. Geometric feasibility enforces manufacturability requirements: minimum thicknesses not below the lamination thickness (with a lower bound of 0.25 mm), a minimum magnet dimension of 3 mm, and the inclusion of features such as chamfers, magnet pockets, and corner roundings (Fig. 1). These elements reflect real production constraints and affect both stress distribution and electromagnetic behavior. Material usage is limited by a maximum magnet mass of $1.6,\text{kg}$, slightly above the precursor value (Table I), allowing limited refinement without significant increases.

2) Second level: is applied only when the mechanical solver is disabled (MECH-OFF). In this case, minimum thickness constraints are imposed on the inner and outer bridges of each magnet layer, derived from a preliminary structural analysis of the precursor design. These limits act as conservative surrogate checks to exclude non-robust configurations. Given the nonlinear and geometry-dependent nature of the structural response, such constraints do not ensure mechanical integrity but approximate feasibility in the absence of explicit analysis. When mechanical screening is enabled (MECH-ON), these limits are removed and structural admissibility is evaluated directly via finite element analysis.

For each candidate solution, the parametric design routine is executed with an embedded repair procedure [18]. This operates directly on the design variables, resolving geometric violations while preserving the generated configuration. Violating variables are randomly remapped within admissible bounds, acting as a mutation-like correction step.

When MECH-OFF is active, the repair enforces both constraint levels, including bridge-thickness limits as a surrogate for structural feasibility. When MECH-ON is active, it is restricted to first-level constraints, leaving mechanical integrity entirely to the in-loop FEM evaluation.

As shown in Fig. 2, only candidates with a valid geometry proceed. With MECH-ON, they undergo structural analysis (Section III-D); otherwise, they are directly evaluated for rotor THD.

D. In-Loop Mechanical Simulation

This subsection describes the finite-element mechanical evaluation replacing surrogate constraints, including the solver, structural model, and admissibility criterion. When MECH-ON is active, this analysis is performed after geometry validation and before electromagnetic evaluation. The open-source solver CalculiX (CCX) [19], [20] is used to enable efficient parallel execution.

Mechanical screening is based on a stress criterion under overspeed conditions, set to 110% of the maximum operating speed according to stamdard GB/T 18488–2024 [21]. At this speed, loss of shaft–rotor interference is assumed. The maximum allowable stress is fixed at 420 MPa based on the rotor material properties.

1) Structural Model Implementation: The pre-processing pipeline includes: (i) geometry generation, (ii) triangular meshing using `triangle.exe` [22], consistent with the electromagnetic FEMM discretization, and (iii) MATLAB-based preprocessing with CCX input generation.

For each feasible geometry, the structural model is defined by enforcing a *tie* constraint at the magnet–rotor interface. Magnets are not explicitly meshed; only the rotor iron is discretized. Their centrifugal effect under overspeed is modeled through equivalent nodal loads applied along the interface, scaled by the associated segment length. This approach ensures weak dependence on mesh density and consistent load transfer.

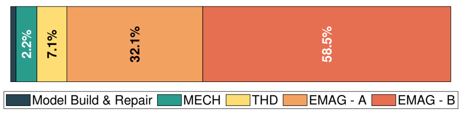

Fig. 3. Mean execution time measured over 100 complete fitness evaluations using 20 parallel instances. Simulations were performed on an Intel Core i9-14900K @ 3.2 GHz, 64 GB DDR5-4000 RAM (4 × 16 GB), and a 512 GB Samsung PCIe NVMe M.2 SSD.

The CCX input file is generated in MATLAB and defines nodes, CPS3 plane-stress elements, nonlinear material properties, centrifugal body loads on the rotor-iron mesh, and equivalent nodal loads at the magnet–rotor interface. Symmetry is enforced by constraining the tangential displacement on the pole symmetry planes. The problem is solved as a static analysis using the direct `PaStiX` solver, with a maximum of 30 increments to limit runtime in critical cases.

These modeling choices balance accuracy and computational cost. For meshes of about 20,000 nodes, structural evaluation accounts for roughly 2.2% of the total fitness time, thus introducing a limited overhead (Fig. 3). Additionally, mechanically inadmissible designs are discarded before electromagnetic analysis (Fig. 2), avoiding the most expensive evaluation stage.

2) Post-processing and Admissibility Criterion: Post-processing is performed in MATLAB by parsing the CCX `.frd` output. Nodal von Mises stresses are combined with the geometric parameterization to identify overstressed regions, defined as clusters exceeding $\sigma_{\text{lim}} = 420\ \text{MPa}$, and classified by location within the rotor. Clusters are analyzed in: (i) rotor–shaft interface, (ii) outer magnet barriers, (iii) inner magnet barriers, and (iv) mass-reduction holes.

The overstressed area is evaluated by identifying nodes with $\sigma_{\text{vM}} > \sigma_{\text{lim}}$, retrieving their neighbors through inverse connectivity, and confirming them only if the average stress of adjacent nodes lies within -2% of σ_{lim} to remove numerical artifacts. The areas of connected elements are then accumulated without duplication, assigned to geometry-based clusters, and compared against cluster-specific tolerances, with only exceeding contributions summed into the total overstressed area A_{os}.

A candidate geometry is considered mechanically admissible if $A_{\text{os}} = 0$; otherwise, it is classified as non-admissible, discarded prior to electromagnetic evaluation, and penalized proportionally to A_{os} (Table III). Figure 4 illustrates a non-admissible case, where overstressed elements are clustered by magnet layer and barrier side, and their accumulated area defines the penalty.

The proposed post-processing strategy and admissibility definition not only support the current screening approach, but also provide a structured basis for future geometry-repair and mesh-level topology-optimization extensions.

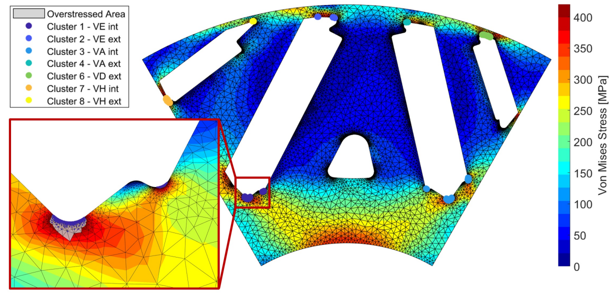

Fig. 4. Mechanically non-admissible candidate rejected during in-loop screening at 110% overspeed. The total overstressed area is $A_{\text{os}} = 0.1955\text{mm}^2$. Grey regions indicate elements exceeding the stress limit, while colored markers denote clusters classified by magnet layer and barrier side.

E. Penalty Function and Low-Performance Handling

Building on the defined constraint architecture and mechanical screening, the fitness evaluation applies staged rejection gates, with penalties summarized in Table III and the full sequence shown in Fig. 2.

Candidates passing all rejection gates proceed to electromagnetic evaluation. A no-load THD analysis is first performed; if THD exceeds 20%, the candidate is rejected. Otherwise, full electromagnetic simulations are carried out and performance thresholds are applied: $T_{\text{nom}} > 265, \text{Nm}$ and $T_{\text{rip}} < 25\%$. Solutions violating these limits are classified as underperforming and penalized accordingly.

For each objective i, a violation δ_i is defined as the distance from the corresponding performance threshold:

$$\delta_i = \max(0, s_i - b_i) \quad (4)$$

where s_i is the objective score and b_i the corresponding threshold. To account for different scales, violations are normalized, and the penalty contribution π_i for objective i is defined as:

$$\pi_i = w_i \left(\frac{\delta_i}{b_i} \right)^{p_i} \quad (5)$$

where w_i is the weight of the i-th objective and p_i controls penalty nonlinearity. A linear formulation is here adopted ($p_i = 1$). Weights are set to $w_i = 1$ for ripple objectives and $w_i = 4$ for torque, to favor high-torque solutions. The aggregated penalty P_a is then obtained by summing all contributions:

$$P_a = \sum_i \pi_i \quad (6)$$

Finally, P_a is added to the objective scores of candidates with severe underperformance in at least one objective. This discourages solutions that are competitive on a single objective but poor on others, which is critical in a narrow high-performance design space.

IV. Results and Discussion

The proposed approach is validated through 10 optimization runs with and without in-loop mechanical screening

TABLE III. Penalty handling

Condition	Penalty factor	Description
Repair Range error	10^6 + 5 × Range Violation	Occurs if repair fails because at least one parameter cannot be remapped to a feasible region
Overlapping area	10^5 + 5 × Overlap Area	Occurs when the magnets of two different layers overlap
Over Weight	10^4 + 5 × Mass Value	Occurs if the total magnet mass exceeds 1.6 kg
Over Stress	10^3 + 5 × Total Overstressed Area	Occurs if at least one cluster's overstressed area exceeds the threshold
Over THD	10^2 + THD Value	Occurs when the THD exceeds 20%
Underperformance	$10 + P_a$ + i-th Objective Score	Occurs when the score does not meet the minimum performance requirement

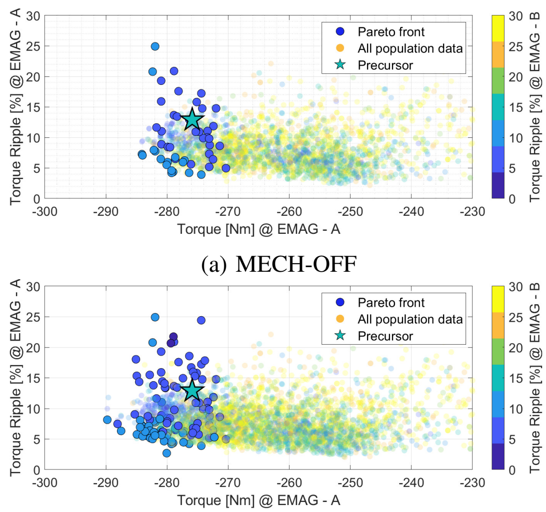

(a) MECH-OFF

(b) MECH-ON

Fig. 5. Objective-space distribution and resulting Pareto front for (a) the MECH-OFF optimization run and (b) the MECH-ON optimization run. All the evaluated individuals is shown with semi-transparent markers, whereas the Pareto-optimal solutions are highlighted with opaque markers. The star denotes the initial precursor design.

(MECH-ON vs. MECH-OFF). To assess physical realizability, the MECH-OFF Pareto set is re-evaluated using the same structural model. On average, 32 out of 100 Pareto-optimal solutions are rejected, confirming that electromagnetic-only optimization can produce partially non-implementable fronts under structural constraints.

Figures 5a and 5b compare the final Pareto fronts, with the MECH-OFF front shown after post-convergence structural screening. The plots report torque ripple versus average torque at EMAG-A, with color indicating ripple at EMAG-B. The MECH-ON configuration has a lower feasibility rate: as shown in Fig. 6, the mean number of infeasible evaluations increases from 2521 to 3911, as in-loop screening rejects electromagnetically promising but mechanically unfeasible designs.

Despite the higher rejection rate, the MECH-ON Pareto set shifts toward a more favorable trade-off region. This is due to the different constraint handling: without mechanical simulation, conservative geometric limits are required to ensure safety, whereas with in-loop evaluation these constraints are removed, retaining only essential ones. The design space is thus less restricted, allowing solutions that exploit the material closer to its structural limit and avoid over-dimensioning.

The presence of inadmissible solutions in the MECH-OFF Pareto front makes a-posteriori filtering ineffective: since such solutions influence convergence, mechanical screening must act as an active constraint within the evolutionary process rather than as a post-processing step.

The MECH-ON Pareto set enables direct, physically consistent design selection. Since the objectives capture only part of the system behavior, additional indicators – such as torque-to-magnet-mass ratio, THD, and ripple at both operating points – must be jointly considered. Fig. 7 summarizes three representative trade-off solutions against the precursor, with axes oriented so that larger values denote better performance. The selected solutions reflect different design strategies. TradeOff01 maximizes peak torque (+15 Nm) with limited ripple, at the cost of increased magnet mass. TradeOff02 maintains magnet mass below the precursor while reducing ripple at EMAG-A by 61%, providing a balanced compromise. TradeOff03 maximizes torque-to-magnet-mass ratio, reducing magnet mass by over 200 g with a 7 Nm torque penalty, favoring cost- and weight-sensitive applications.

In all cases, the availability of structurally admissible solutions with improved electromagnetic performance confirms that in-loop mechanical screening supports more informed and physically consistent design decisions.

V. Conclusion

This work presents a multiphysics, multi-objective optimization framework for IPMSM rotor design, coupling evolutionary search with in-loop mechanical screening. Electromagnetic performance is evaluated via FEMM, while structural admissibility is enforced through CCX, enabling the rejection of mechanically infeasible designs. This integration alters both feasibility statistics and the resulting Pareto set, allowing the exploration of high-performance configurations without conservative surrogate constraints. The optimized solutions achieve improved electromagnetic performance at comparable or reduced magnet mass, indicating more efficient material use. Future work will extend the approach toward mesh-level optimization, using cluster-based overstress maps to guide localized material redistribution and provide a finer refinement layer.

Acknowledgment

The authors thank Mavel EDT (Italy) for technical support, engineering know-how, and for the specifications used in this work.

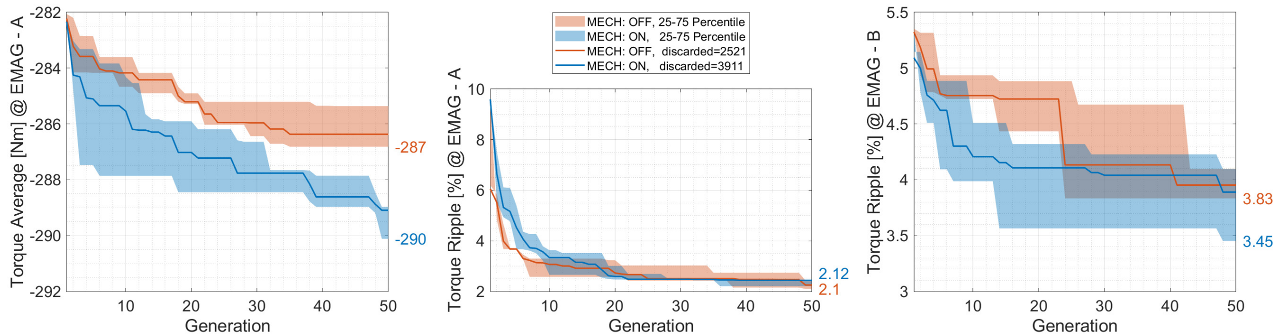

Fig. 6. Convergence curves comparing the optimization without (MECH-OFF) and with in-loop mechanical screening (MECH-ON) over 10 runs. From left to right: torque average, torque ripple at EMAG-A, and ripple at EMAG-B. The legend reports the number of unfeasible candidates discarded; annotated values indicate the best (final) achieved metrics.

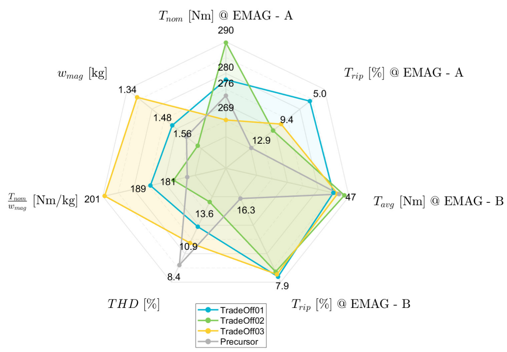

Fig. 7. Radar chart comparing three Pareto-optimal solutions with the precursor design. For radial axes outward directions indicate improved performance.

REFERENCES

[1] M. Gobbi, A. Sattar, R. Palazzetti, and G. Mastinu, "Traction motors for electric vehicles: Maximization of mechanical efficiency–a review," *Applied Energy*, vol. 357, p. 122496, 2024.

[2] M. F. B. Omar, E. B. Sulaiman, I. A. Soomro, M. Z. B. Ahmad, and R. Aziz, "Design optimization methods for electrical machines: A review," *Journal of Electrical Engineering & Technology*, vol. 18, no. 4, pp. 2783–2800, 2023.

[3] X. Sun, B. Wan, G. Lei, X. Tian, Y. Guo, and J. Zhu, "Multiobjective and multiphysics design optimization of a switched reluctance motor for electric vehicle applications," *IEEE Transactions on Energy Conversion*, vol. 36, no. 4, pp. 3294–3304, 2021.

[4] S. Tosun, "The design of the outer-rotor brushless dc motor and an investigation of motor axial-length-to-pole-pitch ratio," *Sustainability*, vol. 14, no. 19, 2022.

[5] S. Zheng, X. Zhu, L. Xu, Z. Xiang, L. Quan, and B. Yu, "Multi-objective optimization design of a multi-permanent-magnet motor considering magnet characteristic variation effects," *IEEE Transactions on Industrial Electronics*, vol. 69, no. 4, pp. 3428–3438, 2021.

[6] C. Zhang, Z. Chen, Q. Mei, and J. Duan, "Application of particle swarm optimization combined with response surface methodology to transverse flux permanent magnet motor optimization," *IEEE Transactions on Magnetics*, vol. 53, no. 12, pp. 1–7, 2017.

[7] X. Zhu, Z. Shu, L. Quan, Z. Xiang, and X. Pan, "Multi-objective optimization of an outer-rotor v-shaped permanent magnet flux switching motor based on multi-level design method," *IEEE Transactions on Magnetics*, vol. 52, no. 10, pp. 1–8, 2016.

[8] H. Chen and C. H. Lee, "Parametric sensitivity analysis and design optimization of an interior permanent magnet synchronous motor," *IEEE Access*, vol. 7, pp. 159 918–159 929, 2019.

[9] L. Balasubramanian, N. A. Bhuiyan, A. Javied, A. A. Fahmy, F. Belblidia, and J. Sienz, "Design and optimization of interior permanent magnet (ipm) motor for electric vehicle applications," *CES Transactions on Electrical Machines and Systems*, vol. 7, no. 2, pp. 202–209, 2023.

[10] S. Barmada, M. Tucci, L. Sani, and C. Tozzo, "Deep neural network-based electro-mechanical optimization of electric motors," *IEEE Transactions on Magnetics*, vol. 59, no. 5, pp. 1–4, 2022.

[11] T.-H. Ji, C.-H. Kim, S.-W. Jung, and S.-Y. Jung, "Design method of ipmsm using multi-objective optimization considering mechanical stress for high-speed electric vehicles," *Journal of Electrical Engineering & Technology*, vol. 19, no. 4, pp. 2481–2489, 2024.

[12] S. Ferrari, L. Solimene, R. Torchio, C. Anerdi, F. Freschi, L. Giaccone, G. Lorenti, F. Lucchinizz, P. Alotto, G. Pellegrino, and M. Repetto, "A multiphysics dataset generation procedure for the data-driven modeling of traction electric motors," *IEEE Access*, vol. 13, pp. 54 534–54 546, 2025.

[13] H. Zhou, X. Wang, L. Xiong, and X. Zhang, "Analysis and research on mechanical stress and multiobjective optimization of synchronous reluctance motor," *CES Transactions on Electrical Machines and Systems*, vol. 8, no. 3, pp. 274–283, 2024.

[14] B. Santoshkumar and K. Deb, "Handling objectives with heterogeneous evaluation times in surrogate-assisted evolutionary multiobjective optimization," *IEEE Transactions on Evolutionary Computation*, vol. 30, no. 2, pp. 564–578, 2026.

[15] K. Deb, A. Pratap, S. Agarwal, and T. Meyarivan, "A fast and elitist multiobjective genetic algorithm: NSGA-II," *IEEE Transactions on Evolutionary Computation*, vol. 6, no. 2, pp. 182–197, 2002.

[16] D. Meeker, "Finite element method magnetics," 2018, [Computer software]. [Online]. Available: https://www.femm.info/wiki/HomePage

[17] D. Meeker, "Finite element method magnetics user's manual, version 4.2," 2018. [Online]. Available: http://www.femm.info/Archives/doc/manual42.pdf

[18] F. Valpiani, M. Biasizzo, A. Niccolai, and S. Leva, "A novel repair function for enhancing parametric design optimization of internal permanent magnet synchronous motors with asymmetric rotor poles," in *2025 25th International Conference on the Computation of Electromagnetic Fields (COMPUMAG)*, 2025, pp. 1–7.

[19] G. Dhondt and K. Wittig, "Calculix: A three-dimensional structural finite element program," 1998–2025, [Computer software]. [Online]. Available: https://www.calculix.de/

[20] G. Dhondt, *The Finite Element Method for Three-Dimensional Thermomechanical Applications*. John Wiley & Sons Inc, 2004.

[21] State Administration for Market Regulation and Standardization Administration of People's Republic of China, "GB/T 18488–2024: Drive motor system for electric vehicles," May 2024.

[22] J. R. Shewchuk, "Triangle: Engineering a 2D Quality Mesh Generator and Delaunay Triangulator," in *Applied Computational Geometry: Towards Geometric Engineering*, ser. Lecture Notes in Computer Science, M. C. Lin and D. Manocha, Eds. Springer-Verlag, May 1996, vol. 1148, pp. 203–222, from the First ACM Workshop on Applied Computational Geometry.